J. Fluid Mech. (1992), *vol.* 244, *pp.* 149–169

Nonlinear waves on the surface of a falling liquid film. Part 2. Bifurcations of the first-family waves and other types of nonlinear waves

By O. Yu. TSVELODUB AND Yu. Ya. TRIFONOV

Institute of Thermophysics, Russian Academy of Sciences, Novosibirsk 630090, Russian Federation, CIS

(Received 12 June 1990 and in revised form 22 April 1992)

The paper is devoted to a theoretical analysis of nonlinear two-dimensional waves on the surface of a liquid film freely falling down a vertical plane. A bifurcation analysis of the wave regimes found in Part 1 of this work (Tsvelodub & Trifonov 1991), and of the new wave families obtained here in Part 2, has been carried out. It is demonstrated that there is a great number of different steady-state travelling wave classes which are parameterized by wavenumber at a fixed Reynolds number for a given liquid. It is shown that some of them quantitatively agree with experimental results. The question of stability of various wave regimes with respect to two-dimensional infinitesimal disturbances is examined and it is shown that one particular wave family is found. The most amplified disturbances are evaluated.

1. Introduction: governing equations and methods used in the stability investigation and in the bifurcation analysis

A discussion of some basic theoretical and experimental results published previously is given in Part 1 of this work (Trifonov & Tsvelodub 1991). Here we state only the governing equations, and review briefly the numerical procedure for finding steady-state travelling waves and the method of the stability investigation given in more detail in Part 1, and discuss some main results of Part 1.

We consider a two-dimensional flow of a viscous incompressible liquid on a vertical plane. A schematic of the flow and the coordinate system are shown on figure 1. We shall consider only long-wave disturbances in terms of the parameter $\epsilon = h_0/L \ll 1$. Here h_0 is the mean film thickness and L is a characteristic scale of length in the x-direction. For the range of Reynolds numbers under consideration

$$\epsilon \ll Re \lesssim 1/\epsilon \ (Re = q_0/\nu,$$

where ν is kinematic viscosity and q_0 is the mean flow rate in a wavy film), after neglecting terms smaller than $O(\epsilon)$, the Navier–Stokes equations and boundary conditions are substantially simplified:

$$\left.\begin{aligned} \frac{\partial u}{\partial t}+u\frac{\partial u}{\partial x}+v\frac{\partial u}{\partial y} &= g+\frac{\sigma}{\rho}\frac{\partial^3 h}{\partial x^3}+\nu\frac{\partial^2 u}{\partial y^2}, \\ \frac{\partial u}{\partial x}+\frac{\partial v}{\partial y} &= 0, \\ u = v = 0, \quad y = 0; \quad \frac{\partial u}{\partial y} &= 0, \quad y = h(x,t). \end{aligned}\right\} \tag{1.1}$$

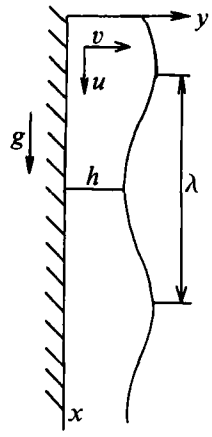

FIGURE 1. Schematic representation of a vertical falling liquid film.

Here g is the acceleration due to gravity, σ is the coefficient of surface tension and ρ is liquid density.

In deriving (1.1) we retain the term for the capillary pressure. It is correct if the film number $Fi = (\sigma/\rho)^3/g\nu^4 \sim Re^5/\epsilon^6$, which is the case in most experiments.

In spite of the assumptions used it is difficult to find wavy solutions of (1.1) and therefore the self-similarity velocity profile assumption was also used:

$$u(x,y,t) = U(x,t)\,(y/h(x,t) - y^2/2h^2(x,t)). \tag{1.2}$$

For long waves this assumption is reasonable but it is extremely difficult to evaluate its correctness mathematically. However, the experimental results and some direct numerical simulations show that this assumption is valid for the values of Reynolds numbers under consideration. The physical correctness of (1.2) may be proved by comparing the solutions of the simplified system with the experimental results.

Substituting the profile (1.2) into (1.1) and integrating over the y-direction from 0 to $h(x,t)$ gives us the following system of equations in dimensionless form:

$$\frac{\partial q^*}{\partial t^*} + 1.2\frac{\partial}{\partial x^*}\left(\frac{q^{*2}}{h^*}\right) = Fh^* - Z\frac{q^*}{h^{*2}} + 3h^*\frac{\partial^3 h^*}{\partial x^{*3}}, \tag{1.3a}$$

$$\frac{\partial h^*}{\partial t^*} + \frac{\partial q^*}{\partial x^*} = 0. \tag{1.3b}$$

Here

$$q^* = \frac{q}{q_0}, \quad h^* = \frac{h}{h_0}, \quad x^* = \left(\frac{3}{We}\right)^{\frac{1}{2}}\frac{x}{h_0}, \quad t^* = \left(\frac{3}{We}\right)^{\frac{1}{2}}\frac{tq_0}{h_0^2},$$

$$Z = \left(\frac{3We}{Re^2}\right)^{\frac{1}{3}}, \quad F = \left(\frac{We}{3Fr^2}\right)^{\frac{1}{3}}, \quad We = \frac{\sigma h_0}{\rho q_0^2}, \quad Fr = \frac{q_0^2}{gh_0^3}, \quad q = \int_0^h u\,\mathrm{d}y$$

(q is the flow rate of the film liquid).

To find periodic nonlinear steady-state travelling solutions of (1.3), $h^* = h^*(\xi)$, $q^* = q^*(\xi)$, $\xi = x - ct$ (c is the phase velocity), it is convenient to use the wavelength-averaged thickness and flow rate as scales of h and q respectively. This choice of scales is more suitable for comparing the calculated and experimental results. As a rule, the

Reynolds number based on the mean liquid flow rate is a natural and well-controlled parameter for experiments on waves travelling down a liquid film and the results are often represented as functions of this parameter. For such a choice of scales the relation between h_0 and q_0 is not known beforehand. Therefore, in (1.3) we may fix only one of the two parameters, F or Z. The other one may be determined from the solution. Here the parameter Z will be the one that is fixed.

Now the solution of (1.3) related to Nusselt smooth flow is

$$h^* = 1, \quad q^* = 1, \quad F = Z$$

and a solution exists for any value of Z. To investigate its stability with respect to infinitesimal disturbances,

$$h^* = 1+h', \quad q^* = 1+q', \quad (h', q') \sim \exp[\mathrm{i}\alpha(x^*-c_1 t^*)],$$

the system (1.3) is linearized with respect to h', q' and it is not difficult to obtain the resolving condition for the complex phase velocity c_1 as a function of real parameters α (wavenumber) and Z. If $\mathrm{Im}\,(c_1) > 0$ the disturbance is amplified and if $\mathrm{Im}\,(c_1) < 0$ it disappears. The analysis carried out in Part 1 showed that for any Z there is a neutral wavenumber $\alpha_n = 1$ such that all disturbances with $\alpha < \alpha_n$ are unstable and those with $\alpha > \alpha_n$ disappear. The phase velocity of a neutral disturbance c_n is equal to 3.

Steady-state travelling periodic solutions of (1.3) with finite amplitude are found numerically. The details of the algorithm are given in Part 1 and here we only review briefly the method. For solutions $q(\xi)$, $h(\xi)$, $\xi = x-ct$ (the asterisk being omitted) equation (1.3*b*) becomes $q(\xi) = 1+c(h(\xi)-1)$ and now we have only to obtain the ordinary differential equation for the unknowns $c, F, h(\xi)$.

The periodic wave with wavenumber α is presented as a Fourier series:

$$h = \sum_{n=-\infty}^{\infty} H_n \exp[\mathrm{i}\alpha n\xi], \quad H_n = \bar{H}_{-n}. \tag{1.4}$$

The bar denotes complex conjugation and, due to the norm conditions, $H_0 = 1$.

Taking into account the first $\frac{1}{2}N$ harmonics in the set (1.4), and substituting these into the equation we obtain a system of $N+1$ complex equations for the real unknowns F, c and N complex $(H_{\pm 1}, \ldots, H_{\pm N/2})$. The pseudospectral method and the fast Fourier transformation procedure were used to calculate the harmonics of nonlinear terms.

Since (1.3) is invariant to the changes $t \to t+C_1$, $x \to x+C_2$, where C_1 and C_2 are constants, the origin of the coordinates was usually chosen such that $\mathrm{Im}(H_1) = 0$.

Thus the system of algebraic equations is completed and the Newton–Kantorovich method was used to solve it numerically. To reduce the set (1.4) the number of harmonics was taken so as to satisfy the relation

$$|H_{N/2}| / \sup_{|n|<N/2} |H_n| < 10^{-3}.$$

For this purpose the number N had to be varied, depending on the values of α and Z, over the range from 16 to 128. If this relation was satisfied, then the increase in the number of harmonics under consideration did not influence the results of the calculations. Thus, for example, doubling N gave us, in general, variations of the phase velocity c of less than 1%, and similarly for the film thickness $h(\xi)$ at each point $\xi_i = 2\pi i/(\alpha N)$, $i = 1, \ldots, N$.

The numerical algorithm is given in more detail in Part 1. Here we only emphasize that the Newton–Kantorovich method is very effective for solving the nonlinear equations. The main difficulty in this method is to determine an initial approximation that is close enough to the solution. Using the analytically obtained periodic steady-state travelling solutions of (1.3) with wavenumbers close to the neutral ones as an initial approximation and proceeding with a small enough step in the parameters α, Z into the region of linear instability, the steady-state travelling solutions for all values of Z and α under consideration were found successfully in Part 1. For a given value of Z these solutions are parameterized by their wavenumber α, $0 < \alpha < 1$, and this wave family is called the first family. A comparison with the experiments of Kapitza & Kapitza (1949) and Alekseenko, Nakoryakov & Pokusaev (1985) demonstrated good quantitative agreement between this family of waves and the corresponding 'periodic' regimes in the experiments.

Here the initial approximations for the Newton–Kantorovich method are constructed from the results of the stability analysis. In Part 1 this analysis was carried out for various waves of the first family to determine which waves could be found and so which waves ought to be observed in experiments. It was shown that waves of the first family were stable with respect to two-dimensional disturbances only for narrow range of wavenumber values and if the values of the Reynolds number were not large.

Thus, the purpose of this article is to carry out a bifurcation analysis of the first-family waves and to obtain the nonlinear waves of the other types.

The bifurcation analysis is based on the method of stability investigation which is given in detail in Part 1; here we give only main features.

Let $h_0(\xi)$, $q_0(\xi)$ be a periodic solution of (1.3) with wavenumber α. Substituting $h = h_0(\xi) + h'(\xi, t)$, $q = q_0(\xi) + q'(\xi, t)$ into (1.3) and linearizing it we obtain a system of partial differential equations for studying the stability of the steady-state solution $h_0(\xi), q_0(\xi)$.

Since the variable t is not explicitly incorporated into this system the solution may be represented as

$$h = \mathrm{e}^{-\gamma t} h_1(\xi), \quad q = \mathrm{e}^{-\gamma t} q_1(\xi). \tag{1.5}$$

Here the primes denoting the disturbance values are omitted. Then the system of ordinary linear differential equations with periodic coefficients for h_1, q is

$$\hat{\mathrm{L}}\begin{pmatrix} q_1 \\ h_1 \end{pmatrix} = \gamma \begin{pmatrix} q_1 \\ h_1 \end{pmatrix}, \tag{1.6}$$

where $\hat{\mathrm{L}}$ is the matrix operator given in Part 1.

Since the disturbances are initially limited for all values of ξ, solutions of (1.6) which are also limited for all ξ are of particular interest here. It follows from Floquet's theorem that such solutions are of the form

$$h_1(\xi) = \varphi(\xi)\,\mathrm{e}^{\mathrm{i}\alpha Q\xi}, \quad q_1 = \psi(\xi)\,\mathrm{e}^{\mathrm{i}\alpha Q\xi}, \tag{1.7}$$

where φ, ψ are periodic functions of the same period as $h_0(\xi)$, $q_0(\xi)$, and Q is a real parameter. Substituting (1.7) into (1.6) and Fourier transforming we obtain a linear algebraic problem to determine the eigenvalues γ.

Thus the investigation of the stability of periodic steady-state travelling wave solutions $h_0(\xi)$, $q_0(\xi)$ with respect to infinitesimal two-dimensional disturbances is reduced to studying the spectrum of γ for different values Q. The wave is stable if for

any Q all γ have $\mathrm{Re}(\gamma) \geqslant 0$. If for some value of Q even just one eigenvalue γ has $\mathrm{Re}(\gamma) < 0$ then the solution under consideration is unstable. We emphasize here that a few unstable modes may exist for a given value of Q and a few eigenvalues γ_i may have $\mathrm{Re}(\gamma_i) < 0$, $i = 1, 2 \ldots$.

It follows from (1.7) that it is sufficient to consider Q within any interval of unit length, for example $[-0.5; 0.5]$. In Part 1 it was shown that $\gamma(Q) = \bar{\gamma}(-Q)$ and it was sufficient to consider Q within interval $0 \leqslant Q \leqslant 0.5$.

The results obtained for $Q = 0$ show the stability with respect to a special but important class of disturbances: ones that the same period as the wave flow under consideration. In this case one of the solutions of (1.6), (1.7) is readily found analytically:

$$\gamma = 0, \quad \varphi = \frac{\mathrm{d}h_0}{\mathrm{d}\xi}, \quad \psi = \frac{\mathrm{d}q_0}{\mathrm{d}\xi}. \tag{1.8}$$

This result is a consequence of the Andronov–Vitt theorem concerning the presence of at least one zero Lyapunov index for a closed trajectory. To find the other γ at $Q = 0$ the problem was solved numerically like in the general case $Q \neq 0$. It is important to note that besides (1.8) the stability calculations show the existence of the second eigenvalue $\gamma = 0$ at $Q = 0$ for all nonlinear waves under consideration.

As a rule (see Part 1), disturbances with small values of Q are most dangerous when the nonlinear solution $(q_0(\xi), h_0(\xi))$ under consideration is stable with respect to disturbances of the same period ($Q = 0$). Introducing the set of fast and slow variables

$$\xi_0 = \xi, \quad \xi_1 = \epsilon\xi, \quad t_n = \epsilon^n t, \quad n = 1, 2, \quad \epsilon = Q$$

and expanding the unknowns in (1.3) in powers of the small parameter

$$q = q_0 + \epsilon q_1 + \epsilon^2 q_2 + \ldots, \quad h + h_0 + \epsilon h_1 + \epsilon^2 h_2 + \ldots,$$

the analytic method was used to investigate the wave stability with respect to such disturbances.

A non-trivial solution of the system to the first power ϵ is proportional to solution (1.8):

$$q_1 = A\frac{\mathrm{d}q_0}{\mathrm{d}\xi}, \quad h_1 = A\frac{\mathrm{d}h_0}{\mathrm{d}\xi}, \tag{1.9}$$

where A is a function of the slow variables.

From the resolution condition of the non-homogeneous system to the third power in ϵ it follows that $A \sim \exp[-\eta t_1 + \mathrm{i}\xi_1]$ and for $a = \mathrm{Re}(\eta)$ we have (see Part 1)

$$a^2 = -R_x.$$

The value of R_x was determined numerically and was a function of $(q_0(\xi), h_0(\xi))$.

If $R_x < 0$, it is obvious that A increases with time, and the solution q_0, h_0 is unstable. If $R_x > 0$, η has an imaginary value. In this case, it is necessary to consider one more approximation.

Substituting $A \sim \exp[-\eta_1 t_2 - \eta t_1 + \mathrm{i}\xi_1]$ into the linear part of the resolution condition at the fourth approximation we arrive at a linear equation to determine η_1. Substituting for η both solutions of the previous approximation we have two values of η_1: η_1^1 and η_1^2. If $\mathrm{Re}(\eta_1^1)$ and $\mathrm{Re}(\eta_1^2)$ are greater than zero, the initial solution is stable, and if at least one of these real parts is less than zero, it is unstable. A more detailed account of the above-stated method is presented in Part 1.

From (1.5), (1.7) it follows that if at some value of Q a real part of some eigenvalue vanishes then a new wave regime branches from an initial one. Thereby either non-stationary (if $\mathrm{Im}(\gamma) \neq 0$) or stationary (if $\mathrm{Im}(\gamma) = 0$) regimes can be generated. If Q is an irrational number, a two-periodic regime in the ξ-direction is generated.

Thus, in the space of parameters Z, α, Q, stationary regimes bifurcate at points lying on the surfaces

$$\gamma(\alpha, Z, Q) = 0. \tag{1.10}$$

The eigenfunction of the neutral disturbance is used to construct the initial approximation for the Newton–Kantorovich method to obtain a new nonlinear solution in the neighbourhood of the bifurcation point. The numerical algorithm to calculate the spectrum of eigenvalues γ was presented in more detail in Part 1. Here we would only like to emphasize that the procedure for investigating the stability and bifurcations and that for calculating the nonlinear solution supplement each other and the agreement between their results ensures the accuracy of the computer algorithms.

2. Bifurcation lines for the first-family waves

Using the methods and equations described in §1, in Part 1 the nonlinear waves of the first family were found numerically and their stability determined for a wide range of Reynolds number Re and right up to the smallest values of wavenumber α. The branching from smooth flow at the line $\alpha = 1$ is of 'soft' type and waves of this family have a sine-like thickness profile up to $\alpha \approx 0.55$. In the limit $\alpha \to 0$ the wave profile transforms into a series of solitary waves – 'negative' solitons. Here and below the word 'soliton' is an abbreviation for 'solitary wave' and there are no features of solitons in the usual context for solutions of (1.3). A comparison with the experiments of Kapitza & Kapitza (1949), Alekseenko *et al.* (1985) and Nakoryakov, Pokusaev & Alekseenko (1981) demonstrated good quantitative agreement between some waves of this family and experimentally observed 'periodic' regimes. Wave stability calculations with respect to two-dimensional disturbances had shown that the long waves of this family were unstable with respect to disturbances with the same period as that of the wave, which is why these waves were not observed in the experiments.

Using results from Part 1 a bifurcation analysis of first-family waves will be carried out in this article and new types of waves will be found.

The results of the first-family-wave stability analysis at $Z = 10$ are given in figure 2 as an example. For this value of Z the region of waves stable with respect to disturbances of the same period (with $Q = 0$) is $0.516 = \alpha_* < \alpha < 1$. In figure 2 the point α_* is the intersection of curves 6 and 7. Note that in the region of waves stable with respect to disturbances of the same period ($Q = 0$) there are no more than two unstable modes of disturbances with small values of Q. The eigenvalues γ of such disturbances vanish with $Q \to 0$ and $\gamma = 0$ is double valued at $Q = 0$, as was discussed in §1.

In the small region between line $\alpha = 1$ and curve 1 in figure 2 there are two eigenvalues γ_i which have $\mathrm{Re}(\gamma_i) < 0$, $i = 1, 2$. As a consequence there are two unstable modes for the given values of α and $Q \neq 0$. On crossing curve 1 one of these unstable modes becomes stable. The second mode becomes stable after crossing curve 2. In the region between curves 2 and 4 shown hatched in figure 2 all disturbances are stable. The region of waves which are stable with respect to all possible

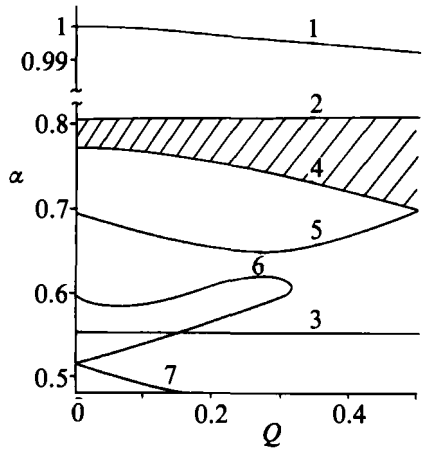

FIGURE 2. Bifurcation lines for solutions of the first family when $Z = 10$. On lines 1–3 $\gamma = 0$ and stationary regimes appear here. On lines 4–7 Re $(\gamma) = 0$ and nonstationary regimes bifurcate here.

disturbances is narrower ($0.772 < \alpha < 0.802$) than that of disturbances with $Q = 0$, which in figure 2, is the intersection of lines 2 and 4 and the axis $Q = 0$. On crossing curve 4 the unstable mode appears again. Also, a stability change of some modes occurs while crossing lines 3, 5–7 in succession.

On lines 1–7 in figure 2 the real parts of some eigenvalues vanish. On lines 1–3 the imaginary parts of the corresponding eigenvalues also vanish, which means that lines 1–3 belong to the surfaces (1.10) and the new steady-state travelling regimes branch from these lines. On lines 4–7 Im $(\gamma) \neq 0$ and the non-stationary regimes bifurcate here.

Analogous bifurcation lines are numerically determined for other values of Z: with decreasing Z they shift towards the region of lower α values. If we number the bifurcation surfaces in the space (α, Q, Z) in accordance with the values of their characteristic wavenumbers then we may say that lines 1–3 in figure 2 the sections of the first three surfaces (1.10) for the $Z = 10$ plane.

3. New families of stationary waves and investigation of their stability

The calculations show that there exist many bifurcation surfaces (1.10) for the first-family waves (e.g. see figure 2). As will be shown, the most interesting solutions in terms of comparison with experiments bifurcate from the first surface (1.10) possessing the highest wavenumbers

$$\alpha = \alpha_{*1}(Z, Q). \tag{3.1}$$

In figure 3, lines 1–3 correspond to the values $\alpha_{\text{new}} = Q\alpha_{*1}(Z, Q)$ when $Q = \frac{1}{2}, \frac{1}{3}, \frac{1}{4}$, respectively. New stationary periodic solutions of system (1.3) with wavenumbers $\alpha = \alpha_{\text{new}}$ (see 1.10) bifurcate along these lines.

Figure 4 makes it possible to imagine more clearly the branching character of the new solutions in the neighbourhood of the bifurcation points. The first-harmonic amplitudes of the wave versus α with increasing distance from the bifurcation area are shown here. Figures 4 (a), 4 (b), and 4 (c) show $Z^{-1} = 0.1$, 1.6 and 0.6, respectively. For figure 4 (a, b) the bifurcation points are on curve 1 of figure 3, for figure 4 (c) it is on curve 2 of figure 3.

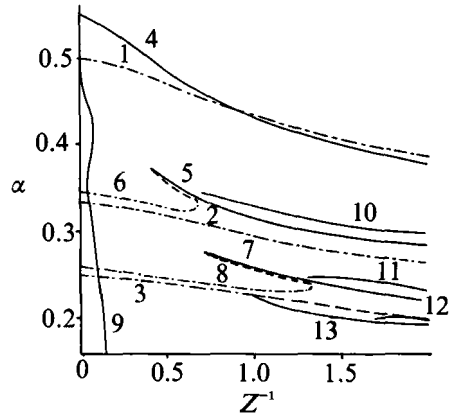

FIGURE 3. New stationary periodic solutions bifurcate along lines 1–3 from the first family. The character of stability with respect to disturbances of the same periodicity changes on reaching line 4. Lines 5–8, 13 are the return lines. Lines 9–12 correspond to Hopf bifurcation.

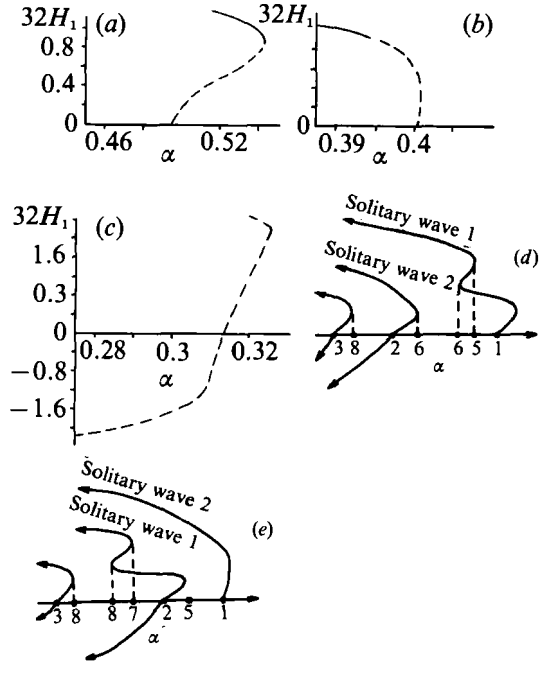

FIGURE 4. The first-harmonic amplitudes of the wave versus α with increasing distance from the bifurcation area. (*a*) $Z^{-1} = 0.1$, the bifurcation point is on curve 1, figure 3; (*b*) $Z^{-1} = 1.6$, the bifurcation point is on curve 1, figure 3; (*c*) $Z^{-1} = 0.6$, the bifurcation point is on curve 2, figure 3. (*d*) The global extension of some local bifurcation curves at $0.4 < Z^{-1} < 0.68$; (*e*) the global extension of some local bifurcation curves at $0.75 < Z^{-1} < 1.33$ (the numbers on the α-axis correspond to the curves in figure 3).

The bifurcation on curve 1 is one-sided. For every value of Z ($Z^{-1} < 2$) the solution first goes to higher α (see figure 4*a*, *b*) and then, after having reached the return line, it shifts towards the region of lower α. Near the bifurcation point this family is unstable with respect to disturbances of the same periodicity ($Q = 0$). The dashed

parts of the curves in figure 4 correspond to such unstable solutions. The character of stability with respect to such disturbances changes on reaching line 4 of figure 3. It should be noted that line 4 in figure 3 does not coincide, at least for $Z^{-1} \geqslant 1$, with the return line (the latter is not shown in figure 3), as it follows from figure 4(*b*).

On curve 2 of figure 3 the bifurcation is two-sided (see figure 4*c*). This case is characteristic of the other curves, including curve 3 in figure 3, corresponding to bifurcations from the surfaces (1.10) at rational numbers of $Q \neq \frac{1}{2}$. For every value of $Z(Z^{-1} < 2)$ both the solutions branching from curve 2 (figure 3) towards the region of lower α and towards the region of higher α (see figure 4*c*) are unstable in the neighbourhood of the bifurcation point with respect to disturbances of the same periodicity ($Q = 0$). The solutions branched towards the region of higher α, and after reaching the return lines 5 or 6 (figure 3) go into the region of lower α. After returning from line 5 these solutions become stable with respect to disturbances of the same periodicity ($Q = 0$).

The branching character of the solutions generated from curve 3 (figure 3) is analogous to that of the solutions generated from curve 2 (figure 3). The bifurcation is two-sided and the branch going to higher α then returns, after having reached lines 7 or 8, towards the region of lower α. On line 7 these solutions become stable with respect to disturbances of the same periodicity ($Q = 0$).

Bunov, Demekhin & Shkadov (1984), when considering some period-doubling bifurcations, presented the basic solution of the first family analytically as a sum of the first two harmonics. The bifurcation points were found by determining real roots of a quadratic equation. Thereby, in the notation used, the bifurcation equation did not have real roots when $Z^{-1} \geqslant 1$ since the basic solution did not bifurcate (i.e. line 1 in figure 3 should terminate when $Z^{-1} \approx 1$). The discrepancy between these results and our calculated data is likely to be related to the fact that over this range of parameters the basic solution cannot be accurately represented by two harmonics.

The new solutions, obtained in the neighbourhood of curves 1–3 (figure 3) were extended throughout the parameter region under consideration, i.e. $\alpha \gtrsim 0.15$, $0.5 < Z < 100$. The calculations show that there is a complex interconnection between these solutions. They form many-folded and many-sheeted surfaces on the plane of parameters α, Z^{-1}.

The calculations show that all branches of solutions appearing on lines 1, 2, 3 (figure 3) continue to the smallest values of α at all fixed values of Z. The limits of these branches as $\alpha \to 0$ are the various solitary waves. For some of these branches there are regions of Z where moving along α forms a fold. Thus the solutions branching from line 1 for $0.4 < Z^{-1} < 0.68$, having reached the upper part of line 6 return to line 5 and move again to the region of small α. The solution branch generated from line 2 towards the region of higher α at $0.75 < Z^{-1} < 1.33$ has an analogous fold between line 7 and the upper part of line 8. These branches of solutions become stable with respect to disturbances with $Q = 0$ on lines 4, 5, 7 as was discussed above. The new stability loss with respect to such disturbances occurs on lines 10, 11, 12, respectively.

Moving along Z at a fixed value of α allows us to see a complex interconnection between these branches of solutions. Thus moving along the arbitrary line $\alpha = \text{const}$ situated above the lower part of curve 6 (figure 3) shows that the solutions branching from curve 1 at small values Z^{-1} transform into ones branching from curve 1 at high values of Z^{-1}. In the region between line 5 and the upper part of line 6 we have the above-mentioned fold (increasing α and Z after having passed this fold the solution may again reach curve 1 (figure 3)). If Z^{-1} varies along the line $\alpha = \text{const}$ which does

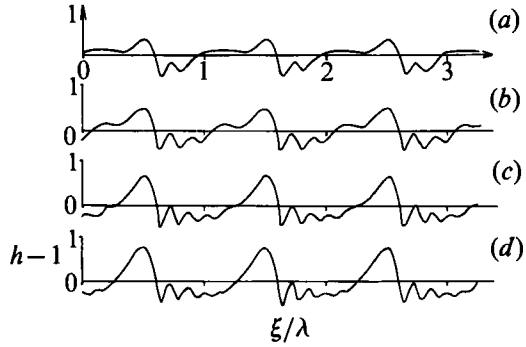

FIGURE 5. Some profiles of the wave thickness for the different families. Here $\alpha = 0.19$, $Z^{-1} = 2$: (*a*) solution bifurcates along line 1, figure 3; (*b*) solution bifurcates along line 2, figure 3, towards higher wavenumber; (*c*) solution bifurcates along line 3, figure 3, towards higher wavenumber; (*d*) solution bifurcates along line $\alpha_{\text{new}} = \frac{1}{5}\alpha_{*1}(Z, \frac{1}{5})$ (see (3.1)).

not intersect curve 6, then curve 5, as earlier, is the return line; however, now the solution extends only up to curve 2. Thus, the solution generated by curve 1 turned out to transform into one of two bifurcation solutions branching from the first family with $Q = \frac{1}{3}$ along curve 2, namely, into the solution which branches towards higher α (see figure 4*c*). If the solutions branching from curve 2 towards higher α at $Z^{-1} < 0.68$, after having turned from line 6 (figure 3), are continued with increasing α and Z^{-1} without the second intersecting of curve 6 then the curve 1 may be reached again. Thus, for all the points on curve 2 (figure 3) the solution bifurcating towards higher α merges, though in a complicated way, with that bifurcating from curve 1.

In the region between the lower part of curve 6, the part of curve 5 where $Z^{-1} > 0.68$, the lower part of curve 8 and the part of curve 7 where $Z^{-1} > 1.33$ we have three different branches of solutions at a given value of Z^{-1} which merge one with another while Z^{-1} varies.

In the region below curve 3 (figure 3) we have at least five different branches (two branches appear on curve 3 and three branches continue in this region from lines 1, 2) and here the merging of these branches one with another, while Z^{-1} varies, occurs too.

Figures 4(*d*) and 4(*e*) make it possible to understand more clearly the description of figure 3 given above. They show the qualitative behaviour of some branches with increasing distance from the bifurcation area. Figure 4(*d*) shows the behaviour of these branches at $0.4 < Z^{-1} < 0.68$ and figure 4(*c*) shows that at $0.75 < Z^{-1} < 1.33$. Here the numbers on the α-axis correspond to the numbers on curves in figure 3.

Thus, even for the first surface (1.10) the branching along the lines corresponding to the first maximum rational values of Q belonging to the interval $[0; 0.5]$ results in the formation of many new steady-state travelling solutions which are interconnected in a rather complicated manner. With decreasing α this process becomes even more complicated, since this is accompanied by concentration of bifurcation lines (as is seen from the comparison between curves 1, 2 and curves 2, 3 in figure 3) and the number of solutions quickly increases. Besides, for small α other surfaces (1.10) begin to manifest themselves and the first wave family generates its own set of solutions on each of them.

The wave film thickness profiles for some of the types of solutions considered above are shown in figures 5–7. In figure 5 the parameters for all regimes are $\alpha = 0.19$, $Z^{-1} = 0.2$. All solutions in figure 5 were obtained by continuously moving along α from the corresponding bifurcation point at a fixed value of Z. The solution

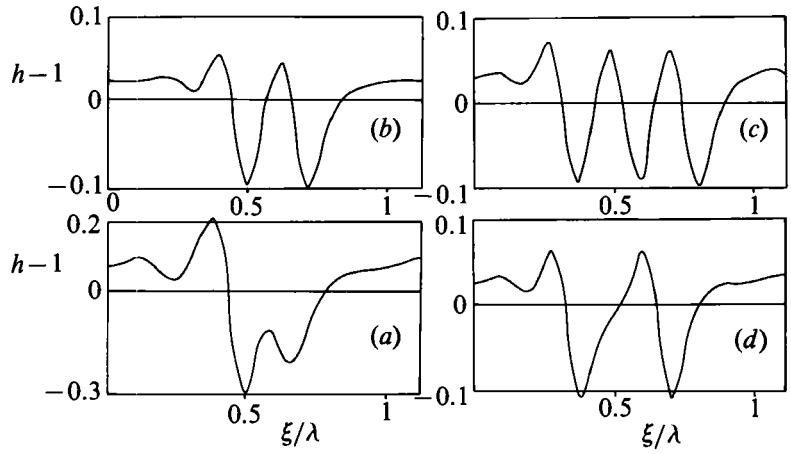

FIGURE 6. Some profiles of the wave thickness for the different families: (*a*) $\alpha = 0.2$, $Z^{-1} = 0.6$. The solution bifurcates along line 2, figure 3, into the region of lower wavenumbers (see figure 4*c*). (*b*, *c*) $\alpha = 0.2$, $Z = 10$. The solutions bifurcate from the second surface (1.10) along line 2, figure 2, for $Q = \frac{1}{2}$ and $\frac{1}{3}$ respectively. (*d*) $\alpha = 0.2$, $Z = 10$. The solution bifurcates from the third surface (1.10) along line 3, figure 2, for $Q = \frac{1}{2}$.

corresponding to figure 5(*a*) bifurcates along line 1 (figure 3); that corresponding to figure 5(*b*) bifurcates along line 2 (figure 3) towards higher wavenumber; that corresponding to figure 5(*c*) represents bifurcation from line 3 also towards higher wavenumbers; the solution corresponding to figure 5(*d*) represents the bifurcation from line $\alpha_{\text{new}} = \frac{1}{5}\alpha_{*1}(Z, \frac{1}{5})$ (see (3.1)).

Though the profiles displayed in figure 5 have some qualitative similarity and correspond to the long waves observed in the experiments there is a rather significant quantitative difference between the waves.

Figure 6(*a*) shows the wave profile of the solution bifurcated from line 2 (figure 3) into the region of lower wavenumbers (see figure 4*b*) for the parameters $\alpha = 0.2$, $Z^{-1} = 0.6$.

Some wave profiles of families bifurcating from the second surface (1.10) along line 2 (figure 2) for $Q = \frac{1}{2}$ and $\frac{1}{3}$ are displayed in figures 6(*b*) and 6(*c*), respectively, and ones bifurcating from the third surface (1.10) along line 3 (figure 2) for $Q = \frac{1}{2}$ are shown in figure 6(*d*). For all these profiles, $\alpha = 0.2$ and $Z = 10$. This wavenumber is rather close to zero and with further decrease in α, Z being fixed, the profiles change slightly, mainly a part of practically horizontal section only is growing. Therefore, it might be expected that as $\alpha \to 0$ these solutions transform into negative solitons with two or three valleys, respectively.

Although a comprehensive numerical analysis of all the solutions is impossible, it may be stated, with some caution, that solutions distinguished in a stability sense, i.e. having different stability properties, are generated on the first bifurcation surface (1.10). Their range of wavenumbers that are stable to disturbances with $Q = 0$ is rather wide. The families, bifurcating from other surfaces (1.10), as was shown by selected calculations, are unstable with respect to disturbances having the same period for all values of α and Z under consideration.

The rather complicated hierarchy of the above-mentioned solutions, bifurcating from the first family, is not complete, since for them there also exists the surface of the type (1.10) over which some of eigenvalues γ pass through zero and new solutions appear. Figure 7 shows the wave profile of one of the families generated due to a

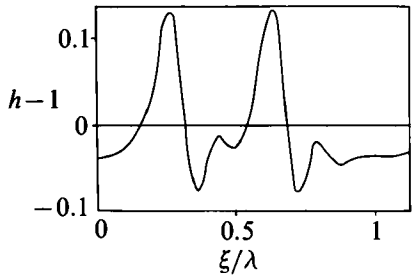

FIGURE 7. The wave profile of a solution which bifurcated from the second family is shown: $\alpha = 0.2$, $Z = 10$.

secondary bifurcation. As in figure 6, here $\alpha = 0.2$, $Z = 10$. This solution is likely to have a limit as a double-humped soliton. Multi-humped-soliton solutions for the equation describing the disturbances on a film when $Re \lesssim 1$ were obtained by Pumir, Manneville & Pomeau (1983). It follows from the above that further bifurcations of the solutions that appear are also available.

Stationary waves divide the area of all periodic solutions into regions behaving in a different manner. The structure of stationary solutions of (1.3) has been shown to be extremely complicated, therefore it is obvious that without this information the evolution of periodic disturbances is impossible to investigate in detail, since for fixed values of α and Z slight variation in the initial data will result in a significant difference in the disturbance evolution. It is also obvious that the presence of a high number of unstable stationary solutions for sufficiently small α will lead to, with high probability, a stochastic behaviour of disturbances for every Z (or, correspondingly, for every Re). The stochastic behaviour of some disturbances for an equation valid for $Re \lesssim 1$ was demonstrated by Shlang & Sivashinsky (1982) and Chang & Chen (1986).

4. Strongly nonlinear waves of the second type, their stability and comparison with experiments

As was shown in §3, solutions exhibiting different stability properties bifurcate from the first surface (1.10). With rational $Q = p/r$, different one-parameter families of the waves bifurcate from the first family on this surface at a fixed value of Z and, as was shown in §3, they are interconnected and form a many-folded and many-sheeted surface on the (α, Z^{-1})-plane (see figure 3).

Waves stable to disturbances of the same period ($Q = 0$) are useful in terms of experimental realization. These solutions, as the calculated results show, behave as if they were on the upper sheet of the surface (figure 3). This sheet represents a continuous extension in α and Z^{-1} of the solution bifurcating from line 1 (figure 3) at small Z^{-1}. Thereby, in this case it is necessary to bypass lines 4, 5, 7, ... Further, taking into account that this definition is restricted, the solutions lying on the upper sheet will be called the second wave family. This second family differs from the first wave family in that it is not a one-parameter family at all values of Z, owing to existence of folds (lines 4, 5, 7, ..., in figure 3).

The definition of the second wave family is difficult: figures 8–13 make it more clear. The characteristics of waves belonging to the second family are shown on these figures by solid parts of lines. The broken lines correspond to solutions which are

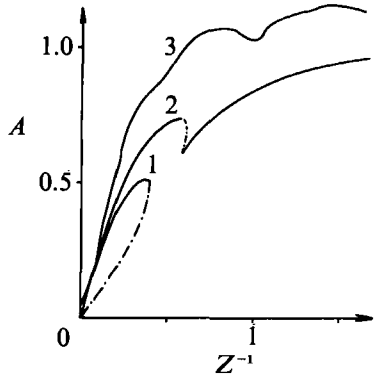

FIGURE 8. Amplitude *vs.* Z^{-1} for the second-family waves: curve 1, $\alpha = 0.5$; 2, $\alpha = 0.35$; 3, $\alpha = 0.2$.

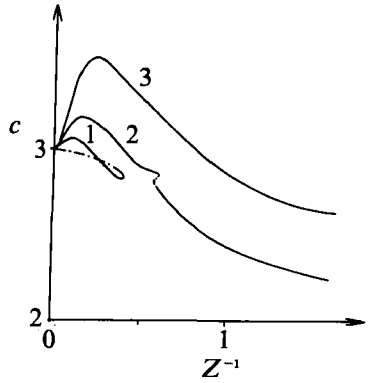

FIGURE 9. Phase velocity *vs.* Z^{-1} for the second-family waves: curve 1, $\alpha = 0.5$; 2, $\alpha = 0.35$; 3, $\alpha = 0.2$.

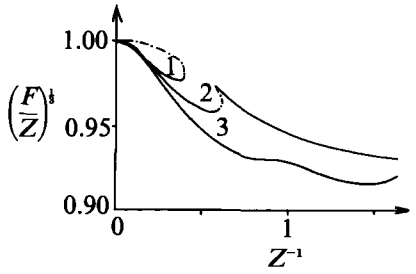

FIGURE 10. Relation between the dimensional mean thickness and the Nusselt thickness (see Part 1, (2.11 *e*)) *vs.* Z^{-1} for the second-family waves: curve 1, $\alpha = 0.5$; 2, $\alpha = 0.35$; 3, $\alpha = 0.2$.

unstable with respect to disturbances with $Q = 0$ and, in accordance with the definition, such solutions are not waves of the second family.

Figures 8–10 display the basic characteristics (amplitude, phase velocity and $(F/Z)^{\frac{1}{3}}$) versus Z^{-1} for three values of the wavenumber. Line 1 is for $\alpha = 0.5$ (the boundary point between the dotted and solid lines is on curve 4 in figure 3), line 2 is for $\alpha = 0.35$ (the broken parts of these curves are connected with the fold between lines 5 and 6 in figure 3), and line 3 is for $\alpha = 0.2$.

For every α value, as seen from figure 3, there exists a Z_{**} at which the solutions intersect lines $4, 5, 7 \ldots$ and then fall into the fold (as in the case with $\alpha = 0.35$ in

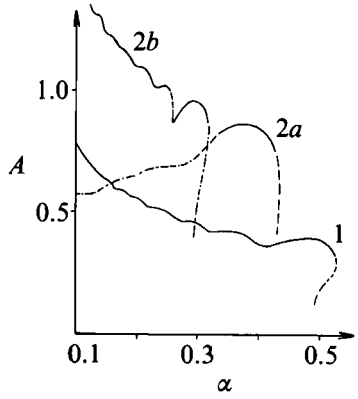

FIGURE 11. Amplitude *vs.* α for the second-family waves: curve 1, $Z^{-1} = 0.2$; 2, $Z^{-1} = 1$.

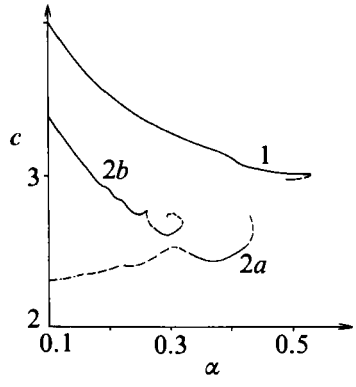

FIGURE 12. Phase velocity *vs.* α for the second-family waves: curve 1, $Z^{-1} = 0.2$; 2, $Z^{-1} = 1$.

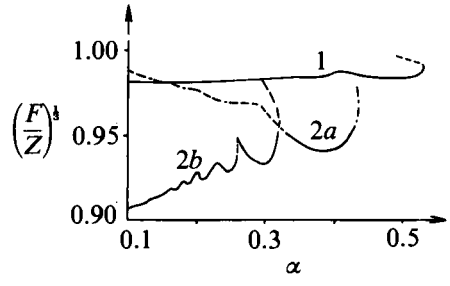

FIGURE 13. Relation between the dimensional mean thickness and the Nusselt thickness *vs.* α for the second-family waves: curve 1, $Z^{-1} = 0.2$; 2, $Z^{-1} = 1$.

figures 8–10), being thereby unstable, or merges with the waves belonging to the first family ($\alpha = 0.5$, figures 8–10). When $\alpha = 0.35$ the solutions, having passed through the fold, again become stable to disturbances with $Q = 0$.

Analogous dependence on the wavenumber α for $Z^{-1} = 0.2$ (line 1) and $Z^{-1} = 1$ (lines $2a$, b) are shown in figures 11–13.

When $Z^{-1} = 0.2$ the solution bifurcates along line 1 (figure 3) from the wave belonging to the first family and becomes stable to disturbances with $Q = 0$ on line 4 (figure 3).

When $Z^{-1} = 1$, the solution bifurcates from line 1 (figure 3) (left-hand broken line $2a$ in figures 11–13): one becomes stable on line 4, and then loses stability again on

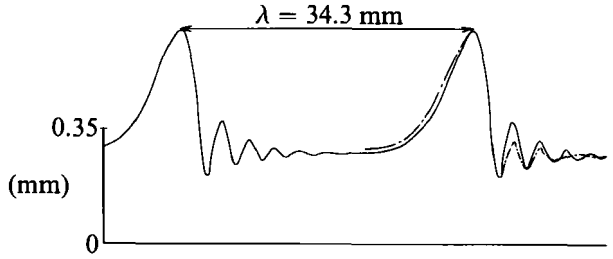

FIGURE 14. Comparison of theoretical (—) and experimental (– – –) thickness profiles for a water–glycerine film: $c_e = 320$ mm/s, $c_c = 318$ mm/s.

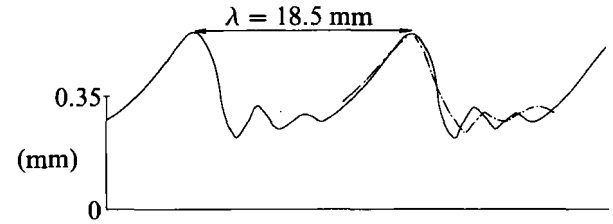

FIGURE 15. Comparison of theoretical (—) and experimental (– – –) thickness profiles for a water–glycerin film: $c_e = 270$ mm/s; $c_c = 262$ mm/s.

line 10 (figure 3); one goes to the other surface sheet in figure 3 (the right-hand broken line $2a$ in figures 11–13). The solution branching from line 2 in figure 3 (first broken portion of line $2b$ in figures 11–13) becomes stable on line 5 in figure 3 with respect to disturbance with $Q = 0$ and then goes to the region of small α. The fold on lines 7 and 8 (figure 3) is shown by the second broken portion of line on curve $2b$ (figures 11–13).

With a decrease in α, the values of A, c, F/Z behave in a rather complicated manner, in contrast to that for waves belonging to the first family (see Part 1). There are some oscillations of the relationships shown in figures 11–13.

Here it should be noted that though the relationships shown in figures 11–13 extend to $\alpha \approx 0.1$, the tendency of F/Z to unity does not manifest itself, the thickness profiles for such α and Z being close to solitary waves (for solitary wave it must be that $F = Z$ as follows from (3.3) of Part 1:

$$F = Z(1/\lambda)\int_0^{\lambda}(1+c(h(\xi)-1))/h^2\,d\xi$$

when $\lambda \to \infty$).

This circumstance is in good agreement with the experimental results obtained by Alekseenko *et al.* (1985), Nakoryakov *et al.* (1981) where, with decreasing frequency of external pulsations, the amplitudes of waves close in form to solitons increased continuously.

Figures 14 and 15 show a comparison between the film thickness profiles experimentally obtained by Nakoryakov *et al.* (1981) (dashed-dotted line) and the calculated profiles of waves belonging to the second family (solid line) for a water–glycerin film with $\nu = 4.9 \times 10^{-6}$ m^2/s, $\sigma/\rho = 59 \times 10^{-6}$ m^3/s^2, $Re = 7.2$. In figure 14, $\lambda = 34.3$ mm, the phase velocity $c_e = 320$ mm/s in the experiment, and $c_c = 318$ mm/s in the calculations. In figure 15, $\lambda = 18.5$ mm, $c_c = 262$ mm/s. $c_e = 270$ mm/s. The dimensionless parameters are $Z^{-1} \approx 1$, $\alpha \approx 0.17$ in figure 14, and $Z^{-1} \approx 1$, $\alpha = 0.31$ in figure 15. It is seen that these values are in good quantitative

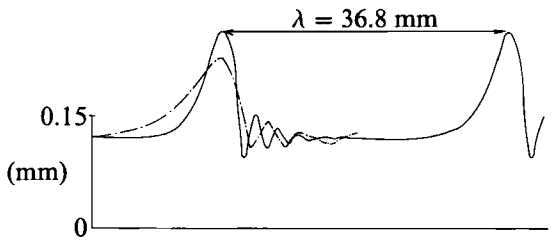

FIGURE 16. Comparison of theoretical (—) and experimental (– – –) thickness profiles for a water film: $c_e = 232$ mm/s; $c_c = 260$ mm/s.

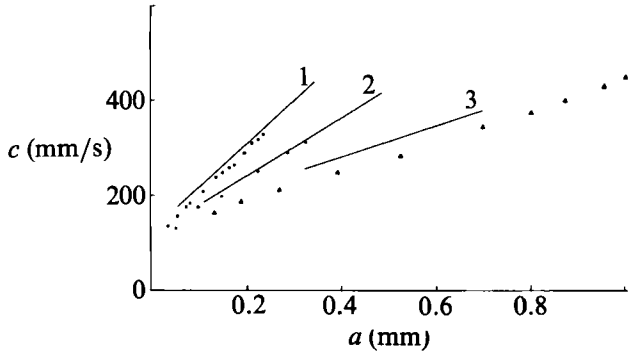

FIGURE 17. Wave velocity *vs.* amplitude. Comparison of the relationships obtained from experiment (—) and from the theory (points). The parameters are given in the text.

agreement. Figure 16 shows an analogous comparison for water ($\nu = 1.03 \times 10^{-6}$ m^2/s, $\sigma/\rho = 72.9 \times 10^{-6}$ m^3/s^2, $Re = 0.8$). Here $\lambda = 36.8$ mm, $c_c = 260$ mm/s, $c_e = 232$ mm/s (the experiment done by Alekseenko 1979). The dimensionless variables are $\alpha \approx 0.13$, $Z^{-1} \approx 0.95$. In this case the experimental and calculated results are in satisfactory agreement.

Here it is necessary to explain how we obtained the correspondence between Re and λ in the experiments and Z, α in the theory. Part 1 contains the relations to recalculate the dimensional wave characteristics and Reynolds number from the dimensionless ones. For example

$$Re = \left(\frac{81Fi}{Z^6}\right)^{\frac{1}{11}}\left(\frac{F}{Z}\right)^{\frac{1}{11}}, \quad \lambda = \frac{2\pi}{\alpha}\left(\frac{\sigma^4\nu^2Z^3}{9\rho^4g^5}\right)^{\frac{1}{11}}\left(\frac{F}{Z}\right)^{\frac{5}{11}}.$$

The value of F here is not known beforehand. Therefore we cannot calculate Z, α from the experimentally measured values of Re, σ/ρ, ν and λ using only these equations. To carry out the comparison these relations were used as just two equations for the main system. The values of Re and λ were fixed and those of Z, α were determined from calculations (as a rough initial approximation the values of Z, α from these equations were obtained by use of the correlation $F = Z$). The dimensional phase velocity and the dimensional profile thickness were calculated after this problem had been solved. The values of α and Z corresponding to Re and λ are given above to two decimal places.

Figure 17 displays a comparison between the experimental and theoretical relationship between phase velocities and amplitudes for the second-family waves. Here the amplitude was determined from the maximum thickness and results are given in dimensional form. Both in the experiment (solid lines) and in the theory (points) the data marked by numbers 1–3 correspond to various waves on the surface

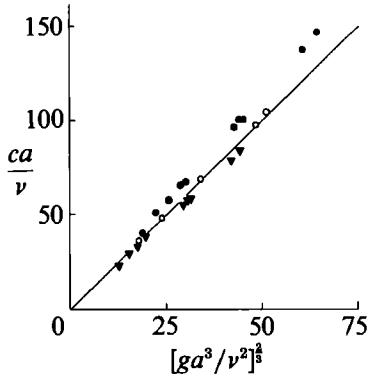

FIGURE 18. Comparison between the best-fit curve for dimensional velocities *vs.* dimensional amplitudes for the experimental data and the results calculated here. The parameters are given in the text.

of a water film ($\nu = 1.03 \times 10^{-6}$ m^2/s, $\sigma/\rho = 72.9 \times 10^{-6}$ m^3/s^2) and of two water–glycerin films ($\nu = 2.06 \times 10^{-6}$ m^2/s, $\sigma/\rho = 40.3 \times 10^{-6}$ m^3/s^2; $\nu = 11.2 \times 10^{-6}$ m^2/s, $\sigma/\rho = 55.9 \times 10^{-6}$ m^3/s^2), respectively. The experimental results are shown by the best-fit solid lines in figure 17 and the data for waves with various wavelengths and at various Reynolds numbers are concentrated in experiments near the corresponding lines with 5–10% dispersion. These results were obtained by Alekseenko (1979). Points 1–3 in figure 17 show the calculated results. These points correspond to various waves of the second family and were obtained at various values of dimensionless parameters α, Z and then, by using the recalculation formulae (see Part 1), the dimensional values of the phase velocity and amplitude for corresponding liquids were found. It is seen that the calculated values are close to the corresponding lines fitted to the experimental data.

Nakoryakov, Pokusaev & Alekseenko (1976) give a simple correlation which generalizes the experimental data on the relationship between the dimensional phase velocities and dimensional amplitudes for various liquids and various strongly nonlinear waves:

$$c = 1.98\,(g^2/\nu)^{\frac{1}{5}}a.$$

Here a is the dimension amplitude determined by the maximum thickness. All experimental data are described by this formula to within 10%. Figure 18 shows a comparison between this curve and the calculated results for the second wave family for different liquids (solid circles, $\nu = 0.9 \times 10^{-6}$ m^2/s, $\sigma/\rho = 72 \times 10^{-6}$ m^3/s^2; open circles $\nu = 1.65 \times 10^{-6}$ m^2/s, $\sigma/\rho = 46.8 \times 10^{-6}$ m^3/s^2; solid triangles, $\nu = 2.12 \times 10^{-6}$ m^2/s, $\sigma/\rho = 28.9 \times 10^{-6}$ m^3/s^2). It is seen that the accordance between the experiment and theory is quite good. We emphasize here once more that in the theory the second-family solutions were obtained at various values of α and Z and the dimensional values of phase velocities and amplitudes were recalculated from dimensionless ones.

Figure 19, taken from Radev (1985), also shows good agreement between our calculations (shown as an open circle) and experimental data (the other four symbols) from Radev (1985), Kapitza & Kapitza (1949) and Nakoryakov *et al.* (1979). The equation for fitting line is

$$c = 2.6\,(Fi^{\frac{1}{11}}kA)^{-0.4}$$

where c, A ($A = h_{\max} - h_{\min}$) are the dimensionless phase velocity and amplitude, $k = 2\pi h_0/\lambda$ and λ is the dimensional wavelength.

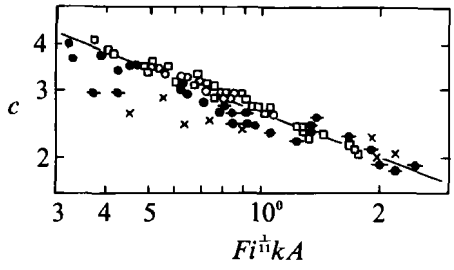

FIGURE 19. Wave velocity *vs.* $(Fi^{\frac{1}{11}}kA)$. Comparison of experiments (●, Radev 1985; -●- Kapitza & Kapitza 1949; ×, □, Nakoryakov *et al.* 1976) and our theory (○).

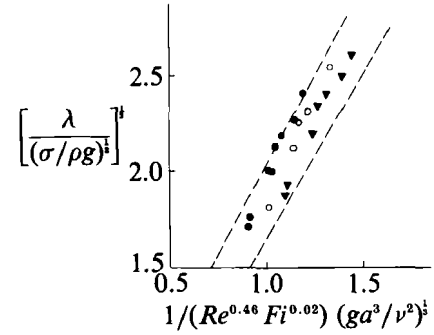

FIGURE 20. A comparison between calculated and experimental data. The experimental data for different liquids fall within the dotted lines. The points denote the numerical results.

The rather wide dispersion of some experimental points in figure 19 is connected with the fact that both fast strongly nonlinear waves and more slow sinusoidal waves of the first family are presented here.

Figure 20 represent a comparison between the calculated and experimental data on the basis of the dependence of the rolling wave amplitude on the wavelength and Reynolds number. It was shown by Nakoryakov *et al.* (1976) that all experimental data for different liquids fall within the dotted lines in figure 20. The three symbols denote the numerical results for waves of the second type for three different liquids with the same properties as in figure 18. These data are also in good agreement with the experiment because they too fall within the dotted lines in figure 20.

Thus the results presented in figures 14–20 allow us to conclude that the nonlinear long waves in experiments correspond to the theoretical second-family waves.

Figure 21 shows the wavenumber stability zones for waves belonging to the second family ($Z^{-1} = 0.1$) and the behaviour of the real parts of the first few eigenvalues of the stability problem (§ 1). As was the case for the waves belonging to the first family, here the stability zones on the (α, Q)-plane are mainly determined by the behaviour of two eigenvalues leaving zero when $Q = 0$. The difference is that now real parts of these eigenvalues oscillate near the axis $\mathrm{Re}\,(\gamma) = 0$ with varying α. As a result the second family has several stability zones. It should be noted also that the absolute value of the increment is lower for the waves belonging to the second family than that for the waves belonging to the first one. This, perhaps, explains why waves belonging to the second family dominate in the experiments. We note here that the plot for $\alpha = 0.26$ illustrates the case when the solution is unstable with respect to disturbances with $Q = 0$ and there are eigenvalues at $Q \to 0$ which are connected with the unstable modes. In figure 3 the solution with $\alpha = 0.26$ is below curve 9.

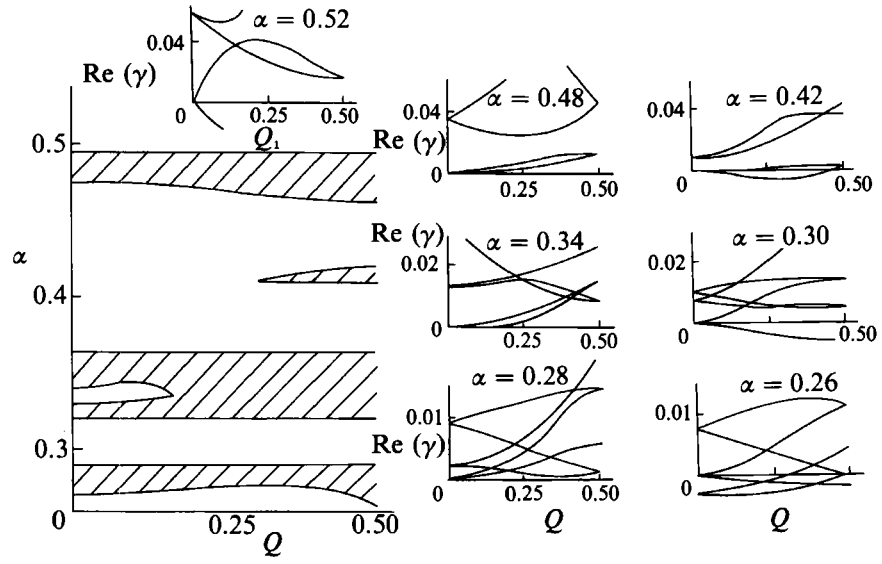

FIGURE 21. Zones of wave regimes stable with respect to disturbances with various Q (shown hatched). The behaviour of the increments of several of the most dangerous disturbances *vs.* Q. is also shown. Here $Z = 10$.

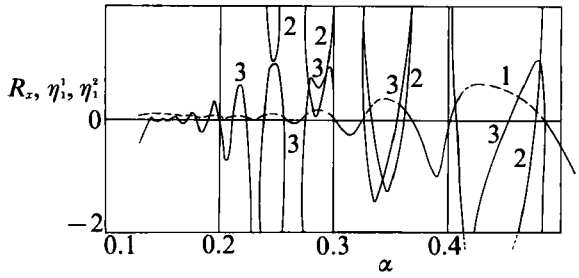

FIGURE 22. Results for the stability of wave regimes with respect to long-modulated disturbances (small Q). Here $Z = 10$. If $R_x < 0$ (line 1) then the disturbances are increasing and the value of the increment is $\sim Q$. If $R_x > 0$ then the stability is determined by values of Re (η_1^1) and Re (η_1^2) (lines 2 and 3), the value of the increment is $\sim Q^2$.

To investigate the stability of wave regimes with small α and increasing Z^{-1} one has to take higher and higher numbers of harmonics to present the basic solution and the possible disturbances. Therefore, in order to save computer time and taking into account that long-modulated disturbances with low Q, as a rule, are the most dangerous, the analytic method described in §1 was used.

The values R_x, Re (η_1^1), Re (η_1^2) for waves belonging to the second family with $Z = 5$ are presented in figure 22: lines 1, 2 and 3 respectively.

If $R_x < 0$ the solution q_0, h_0 is unstable with respect to the long-modulated disturbances. For $R_x > 0$ line 1 is dashed, since at those points the stability is defined by Re (η_1^1) and Re (η_1^2). If Re (η_1^1) and Re (η_1^2) are greater than zero, the solution q_0, h_0 is stable with respect to disturbances with small Q, and if at least one of these real parts is less than zero, it is unstable. It follows from figure 22 that there are several zones of waves that are stable with respect to such disturbances.

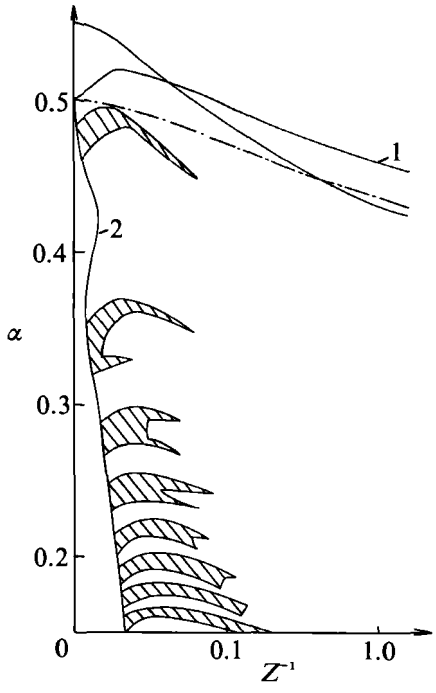

FIGURE 23. Zones of wave regimes stable with respect to long modulated disturbances (small Q), shown hatched. Lines 1, 2 are lines 9, 4 of figure 3.

Figure 23 shows the results of an analytical investigation of waves belonging to the second family for different Z^{-1}. The regions stable to long-modulated disturbances are hatched and adjacent to line 2 (line 9 in figure 3). Line 1 in figure 23 corresponds to line 4 in figure 3.

5. Concluding remarks

The results presented in this article demonstrate a good quantitative agreement between some calculated nonlinear regimes and the experimental data. In contrast to the waves belonging to the first family, these regimes are not a one-parameter family in the universally adopted sense. They form a multi-fold and multi-sheet surface on the (α, Z^{-1})-plane (figure 3). The profiles of nonlinear waves lying on different sheets of this surface are essentially different (figure 7). Owing to the presence of folds and high numbers of harmonics which are necessary to obtain these solutions the authors only succeeded in constructing the surface structure (figure 3) over a restricted region (α, Z^{-1}). Solutions lying on an upper sheet of the surface (figure 3, see §3) that are stable to disturbances of the same period as the period of basic wave may be found. They are conditionally called waves belonging to the second family. The stability of this family to arbitrary plane disturbances is greater than that of the first family. At low values of Z^{-1} the second-family waves have several zones of stable wavenumbers. With increasing Z^{-1} the zones shift towards higher wavelength and become narrower. The instability increments for the waves of this family are lower by an order of magnitude than those for the first one. Therefore, in the experiments waves of this type are likely to be observed throughout the range of wavenumbers where they exist.

REFERENCES

ALEKSEENKO, S. V. 1979 Experimental investigation of two-dimensional wavy flow of liquid film. Ph.D. thesis, Novosibirsk, Institute of Thermophysics.

ALEKSEENKO, S. V., NAKORYAKOV, V. YE. & POKUSAEV, B. G. 1985 Wave formation on a vertical falling liquid film. *AIChE J.* **31**, 1446–1460.

BUNOV, A. V., DEMEKHIN, YE. A. & SHKADOV, V. YA. 1984 Nonuniqueness of wave solutions in viscous layer. *Prikl. Mekn. Mat.* **48**, 691–696.

CHANG, H.-C. & CHEN, L.-H. 1986 Nonlinear waves on liquid film surfaces II. Bifurcation analyses of the long-wave equation. *Chem. Engng Sci.* **41**, 2477–2486.

KAPITZA, P. L. & KAPITZA, S. P. 1949 Wave flow of thin viscous liquid films. *Zh. Teor. Fiz.* **19**, 105–120.

NAKORYAKOV, V. E., POKUSAEV, B. G. & ALEKSEENKO, S. V. 1976 Two-dimensional stationary running waves on a vertically falling liquid film. *Inzh.-Fiz. Zh.* **30** (5), 780–785.

NAKORYAKOV, V. E., POKUSAEV, B. G. & ALEKSEENKO, S. V. 1981 Desorption of weakly-solution gas from flowing liquid films. In *Calculation of Heat and Mass Transfer in Energy-Chemical Processes* (ed. A. P. Burdukov, pp. 23–36. Institute of Thermophysics, Novosibirsk.

PUMIR, A., MANNEVILLE, P. & POMEAU, Y. 1983 On solitary waves running down an inclined plane. *J. Fluid Mech.* **135**, 27–50.

RADEV, K. B. 1985 Dispersion and nonlinearity of waves on a surface of a falling liquid film. In *Fifth Natl Congr. on Theoretical and Applied Mechanics, Sofia*, vol. 2, pp. 745–750.

SHLANG, T. & SIVASHINSKY, G. I. 1982 Irregular flow of a liquid film down a vertical column. *J. Phys. Paris* **43**, 459–466.

TRIFONOV, YU. YA. & TSVELODUB, O. YU. 1991 Nonlinear waves on the surface of a falling liquid film. Part 1. Waves of the first family and their stability. *J. Fluid Mech.* **229**, 531–554.